Quaternary Science Advances 7 (2022) 100054

Contents lists available at ScienceDirect

Quaternary Science Advances

journal homepage: www.sciencedirect.com/journal/quaternary-science-advances

Beryllium isotope variations recorded in the Adélie Basin, East Antarctica reflect Holocene changes in ice dynamics, productivity, and scavenging efficiency

Bethany C. Behrens [a,b,*], Yusuke Yokoyama [a,b,c,d,e,**], Yosuke Miyairi [a], Adam D. Sproson [a,d], Masako Yamane [f], Francisco J. Jimenez-Espejo [d,g], Robert M. McKay [h], Katelyn M. Johnson [h,i], Carlota Escutia [g], Robert B. Dunbar [j]

[a] Atmosphere and Ocean Research Institute, University of Tokyo, 5-1-5 Kashiwanoha, Kashiwa, Chiba, 277-8564, Japan
[b] Graduate Program on Environmental Science, University of Tokyo, Komaba, Meguro, Tokyo, 153-0041, Japan
[c] Department of Earth and Planetary Science, Graduate School of Science, University of Tokyo, Hongo, Bunkyō, Tokyo, 113-8654, Japan
[d] Biogeochemistry Research Center, Japan Agency for Marine-Earth Science and Technology (JAMSTEC), Natsushimacho, Yokosuka, Kanagawa Prefecture, 237-0061, Japan
[e] Research School of Physics, The Australian National University, Acton ACT, 2601, Australia
[f] Institute for Space-Earth Environmental Research, Nagoya University, Furocho, Chikusa, Nagoya, Aichi, 464-8601, Japan
[g] Andalusian Earth Sciences Institute (IACT), CSIC-University of Granada, Armilla, Spain
[h] Antarctic Research Centre, Victoria University of Wellington, Wellington, New Zealand
[i] GNS Science, Lower Hutt, New Zealand
[j] School of Earth, Energy, and Environmental Sciences, Stanford University, Stanford, CA, USA

ARTICLE INFO

Keywords:
Holocene
East Antarctica
Cosmogenic nuclides
Beryllium isotopes
Scavenging

ABSTRACT

The Adélie Basin is a relatively small (~1600 km^2), semi-enclosed continental shelf bathymetric depression located adjacent to the Wilkes Subglacial Basin, a basin underlying a sector of the East Antarctic Ice Sheet that contains ~3–4 m sea level equivalent of ice. Located within the Adélie Basin is a ~184 m thick laminated sediment deposit, the Adélie Drift, ideal for examining regional changes in ice sheet and ocean dynamics. Here, we examine the ratio of reactive beryllium-10 to reactive beryllium-9 ((^{10}Be/^{9}Be)$_{reac}$) in a marine sediment core obtained from the Adélie Drift to assess these changes during the Holocene epoch (11.7 ka BP to present). The (^{10}Be/^{9}Be)$_{reac}$ record provides insight into changes in freshwater input, primary productivity, and scavenging efficiency, while removing the influence of particle size on ^{10}Be concentration. During the early Holocene, (^{10}Be/^{9}Be)$_{reac}$ ratios indicate increased meltwater discharge from ca. 11.7 to 10 ka BP, as grounded ice retreated from the Adélie Basin and adjacent bathymetric highs. After ~10 ka BP, beryllium isotopes are influenced by scavenging efficiency and dilution controlled by ocean currents and accumulation rate, operating alongside meltwater input, suggesting there are additional factors to consider when using (^{10}Be/^{9}Be)$_{reac}$ as a proxy for ice shelf cover and glacial dynamics.

1. Introduction

Antarctic ice sheets contain ~58 m sea level equivalent of ice, ~19 m of which is grounded on bedrock below sea level, as in the Wilkes Subglacial Basin in East Antarctica (Fig. 1A), and is therefore more sensitive to marine ice sheet instabilities triggered by oceanic warming (Thomas and Bentley, 1978; Fretwell et al., 2013; Mengel and Levermann, 2014; Morlighem et al., 2020). Following the Last Glacial Maximum (LGM), Antarctic ice sheet retreat was forced by rising sea level and increased oceanic heat flux (Golledge et al., 2012; The RAISED Consortium, 2014; Fogwill et al., 2017; Yokoyama et al., 2018), at a time of pre-industrial atmospheric CO_2 concentration (~280 ppm; Kemppinen et al., 2018). Atmospheric CO_2 concentration currently exceeds 400 ppm, sea level rise has accelerated from 1.2 ± 0.2 mm yr^{-1} between

* Corresponding author. Atmosphere and Ocean Research Institute, University of Tokyo, 5-1-5 Kashiwanoha, Kashiwa, Chiba, 277-8564, Japan.
** Corresponding author. Atmosphere and Ocean Research Institute, University of Tokyo, 5-1-5 Kashiwanoha, Kashiwa, Chiba, 277-8564, Japan.
E-mail addresses: bethanybehrens@g.ecc.u-tokyo.ac.jp (B.C. Behrens), yokoyama@aori.u-tokyo.ac.jp (Y. Yokoyama).

https://doi.org/10.1016/j.qsa.2022.100054
Received 24 January 2022; Received in revised form 5 April 2022; Accepted 13 April 2022
Available online 18 April 2022

1901 and 1990 to 3.0 ± 0.7 mm yr^{-1} between 1993 and 2010 (Hay et al., 2015), and temperatures in the Southern Hemisphere upper ocean have been increasing since the 1930s (Gille, 2008). With rising sea level and a warming Southern Ocean, constraining the conditions and timing during which the Antarctic ice sheets retreated in the past, and the oceanic response to this retreat, is crucial for informing future ice sheet melting episodes more accurately (e.g., Golledge et al., 2019; Yokoyama and Purcell, 2021).

Modern observations show Wilkes Land, East Antarctica is one of the few regions of the East Antarctic Ice Sheet (EAIS) where retreat has occurred over the past few decades (Miles et al., 2016; Baumhoer et al., 2021). The Wilkes Subglacial Basin catchment (Fig. 1B) contains 3–4 m sea level equivalent of ice which is susceptible to marine ice sheet instability due to its reverse-slope bed (Miles et al., 2018; Mengel and Levermann, 2014; Morlighem et al., 2020). The Adélie Basin is a glacially scoured trough located along the coast of Terre Adélie on the margin of Wilkes Land (Fig. 1) and is influenced by coastal currents, local biological productivity, and outlet glaciers draining the Wilkes Subglacial Basin (Johnson et al., 2021; Expedition 318 Scientists, 2011). After LGM ice retreated, a sediment drift began to form in the Adélie Basin (Expedition 318 Scientists, 2011), the laminated sediment of which provides a unique high-resolution record of sedimentation responding to changes in atmospheric and oceanic circulation, temperatures, and glacial meltwater input throughout the Holocene (Crosta et al., 2018; Ashley et al., 2021; Johnson et al., 2021).

One way to distinguish glacial processes from other factors is by using the cosmogenic isotope beryllium-10 (^{10}Be) produced by interactions between cosmic rays and atoms in the atmosphere (meteoric ^{10}Be) and minerals at the Earth's surface (*in situ* ^{10}Be). Exposure dating of terrestrial rock using *in situ* ^{10}Be has proved a critical tool for constraining the timing of glacial retreat through the dating of glacial landforms such as moraines (e.g., Bentley et al., 2006; Jones et al., 2017; Stone et al., 2003; White et al., 2011; Yamane et al., 2011; Yamane et al., 2015). However, the use of *in situ* cosmogenic nuclides is limited to ice free regions representing ~3% of Antarctica's surface area.

Meteoric ^{10}Be has several applications in glacial environments. It has been measured in ice cores to reconstruct changes in geomagnetic field intensity (Wagner et al., 2000) and solar activity (Pedro et al., 2011), and in sediments to trace depositional processes and evaluate the dynamics of Antarctic ice sheets/ice shelves (Scherer et al., 1998; Yokoyama et al., 2016). An analysis of meteoric ^{10}Be in Ross Sea sediments has been used to track the retreat of both grounded marine ice sheet systems and modern ice shelf systems in the Ross Sea during the middle to late Holocene, with higher recorded concentrations of sedimentary ^{10}Be indicating greater influence of meteoric ^{10}Be under open ocean conditions (Yokoyama et al., 2016).

Despite its successful application, the use of ^{10}Be in bulk sediment is associated with several issues, related to the inability to distinguish which sediment fraction(s) the ^{10}Be is sourced from and the potential influence of sedimentary processes such as particle size, with smaller particles resulting in larger meteoric ^{10}Be concentration (Wittmann et al., 2012; Simon et al., 2016), and scavenging efficiency. Measuring "reactive" ^{10}Be ($^{10}Be_{reac}$) from Fe and Mn oxyhydroxides, which scavenge meteoric ^{10}Be from the water column (Von Blanckenburg and Bouchez, 2014), together with the stable isotope ^{9}Be, sourced from bedrock via weathering, has been demonstrated to provide a reliable approach to correct for these effects (Wittmann et al., 2012). In Antarctica, analyses of marine sediments reveal $(^{10}Be/^{9}Be)_{reac}$ varies across different depositional environments such as sub-glacial, sub-ice shelf, and open marine (Sjunneskog et al., 2007; White et al., 2019). Analysis of Pliocene sediments from offshore Wilkes Land revealed glacial-interglacial variations in $(^{10}Be/^{9}Be)_{reac}$ were derived from meteoric ^{10}Be sourced not only from direct atmospheric deposition during open ocean conditions, but also from ice sheet melt during warm events leading into interglacial periods (Valletta et al., 2018). This is confirmed by a study of $(^{10}Be/^{9}Be)_{reac}$ ratios from sediment cores extracted from Lake Skallen and Lake Maruwan Oike near Lützow-Holm Bay, East Antarctica, which show an increase in $(^{10}Be/^{9}Be)_{reac}$ concentrations at ca. 4.1 ka BP corresponding to late Holocene glacial melt along the Soya Coast (Sproson et al., 2021a).

The timing of grounded ice retreat along the Wilkes Land margin was previously shown in a high resolution ^{10}Be record from the Adélie Basin, Terre Adélie (Behrens et al., 2019). The ^{10}Be data were obtained through whole rock dissolution of sediments (Yokoyama et al., 2019a), constrained by a preliminary age model using novel compound specific radiocarbon analysis (Yamane et al., 2014) that suggest periods of ice sheet retreat may have caused increases in meteoric ^{10}Be at ca. 9.8 ka BP, ca. 6.5 ka BP, and from ca. 4 ka BP. However, since the meteoric ^{10}Be signal may be affected by other variables, such as particle size, which do not reflect environmental forcing mechanisms alone (Wittmann et al., 2012; Simon et al., 2016), measuring the $(^{10}Be/^{9}Be)_{reac}$ in addition to ^{10}Be is vital for recording the history of glacial retreat and/or

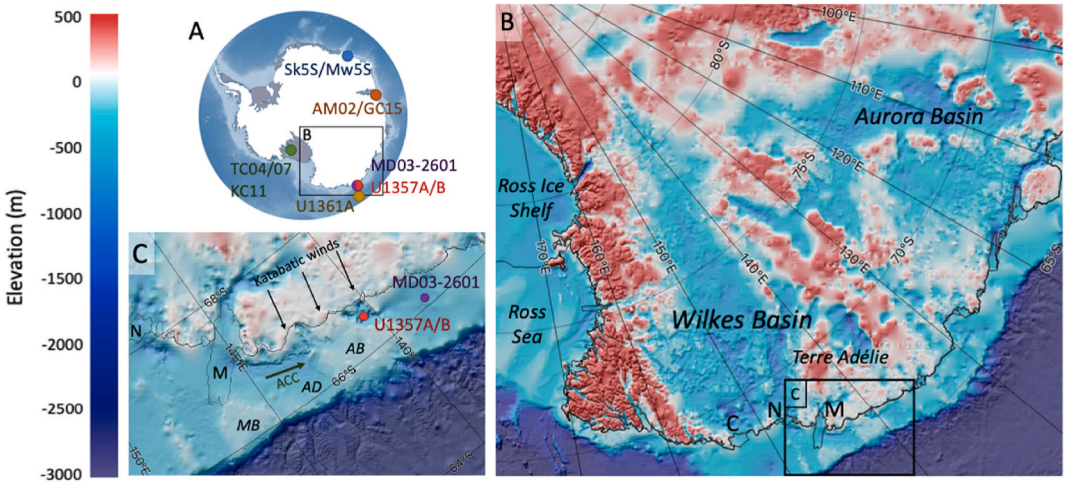

Fig. 1. A) Setting of the Adélie Basin near the Wilkes Basin, locations of Sk5S and Mw5S (blue dot, Sproson et al., 2021a), AM02 and GC15 (brown dot, White et al., 2019), TC04, TC07, and KC11 (green dot, Yokoyama et al., 2016), U1361A (yellow dot, Valletta et al., 2018), MD03-2601 (purple dot, Denis et al., 2009), and U1357A (red dot, this study); B) Bedrock topography in the Wilkes and Aurora basins using the IBCSO elevation model (Arndt et al., 2013); C) hole U1357A and location of hole MD03-2601 (Denis et al., 2009). M, N, and C are used to label the Mertz, Ninnis, and Cook glaciers, respectively. Also labeled are the Adélie Bank (AB), Adélie Depression (AD), Mertz Bank (MB), and the Antarctic Coastal Current (ACC). (For interpretation of the references to colour in this figure legend, the reader is referred to the Web version of this article.)

depositional processes. Here, we analyze $(^{10}Be/^{9}Be)_{reac}$ from the same Adélie Basin marine sediment core as Behrens et al. (2019) to complement the already obtained whole rock ^{10}Be data. These new records are compared with previously published data from Site U1357, local proxy data from core MD03-2601 extracted from the Dumont D'Urville Trough (Fig. 1A), and other $^{10}Be/^{9}Be$ records from around Antarctica (Fig. 1A). To evaluate the timing of ice sheet retreat and related environmental processes such as sea ice cover and biological productivity in the Terre Adélie region of East Antarctica, we will examine three primary processes which potentially affect $^{10}Be_{reac}$ and $^{9}Be_{reac}$ variations in the Adélie Basin: basal melt, increased primary productivity, and changes in the strength of the Antarctic Coastal Current (ACC) and subsequent effects on advection of meltwater and sediment accumulation rate in the Adélie Basin.

2. Regional setting

Terre Adélie is located at 142°E – 136°E between Wilkes Land and George V Land (SCAR, 1992 (updated 2015); Fig. 1B). On the continental shelf at 66°S, 140°E is the Adélie Basin, a glacially scoured 1000 m deep basin separated from the Adélie Depression (~70 km away) by the relatively shallow 200 m deep Adélie Bank (Fig. 1C). The Adélie Basin lies down current of the Mertz Glacier Polynya (MGP), an area of open water with a high rate of sea ice production, brine rejection and associated high primary productivity (Campagne et al., 2015). The main outlet glaciers draining meltwater and sediments offshore and into the Adélie Basin are Zélée, Astrolabe, and Français glaciers, but westward-flowing coastal currents also transport sediment from the Ross Sea and MGP through a trough in the Adélie Bank (Ashley et al., 2021, Fig. 1C). The deep bathymetric configuration of the Adélie Basin and its location adjacent to the Adélie Bank on the inner continental shelf down current of the MGP results in the formation of a sediment drift in the Adélie Basin (Expedition 318 Scientists, 2011). Detrital sedimentation largely results from selective deposition of silts and clays, dependent upon the initial strength of the coastal current as it flows over the bathymetric depression (Fig. 2 of Johnson et al., 2021), while biogenic sedimentation is controlled by seasonally productive diatom blooms that are also advected and concentrated into the drift by these coastal currents (Ashley et al., 2021; Johnson et al., 2021).

3. Materials and methods

Marine sediment from hole U1357A (66°24.7991′S, 140°25.5008′E; Fig. 1C) was collected during the IODP (Integrated Ocean Drilling Program) Expedition 318 at a water depth of 1014.8 m below sea level (mbsl), penetrating to 186 m below sea floor (mbsf) with a core length of 183.87 m. The laminated sediment lies atop a glacial diamict formed during the LGM (Unit III, 185.60 to 185.71 mbsf). Sediment deposited just above the diamict has poorly-sorted sand, clay, and silt content typical of post-glacial retreat, with diatoms composing about 70% of the sediment (Unit II, 170.25 to 185.60 mbsf), which quickly transitions to a laminated diatom ooze with an average diatom content of 90% (Unit I, 0 to 170.25 mbsf) (for more detailed information, see Expedition 318 Scientists, 2011 and Ashley et al., 2021). Here, we measured the $^{10}Be_{reac}$ abundance, $^{9}Be_{reac}$ abundance, and $(^{10}Be/^{9}Be)_{reac}$ composition of sediments above the diamict to ensure the beryllium signal is not affected by local detrital inputs (Tessier et al., 1979; Bourles et al., 1989). Our samples were taken from regular intervals of roughly 800 years to gain insight into the general trend of beryllium isotope variations throughout the Holocene.

Beryllium isotopes are divided into five major fractions or phases: (1) the exchangeable phase, (2) the calcium carbonate phase, (3) Fe and Mn oxyhydroxides, (4) organic, and (5) residual (containing both aluminosilicates and biogenic opal) (Bourles et al., 1989). Phases 1, 2, and 3 are of authigenic origin and contain the "reactive" beryllium. The reactive phase of beryllium was extracted by leaching the sediment with 0.04 M

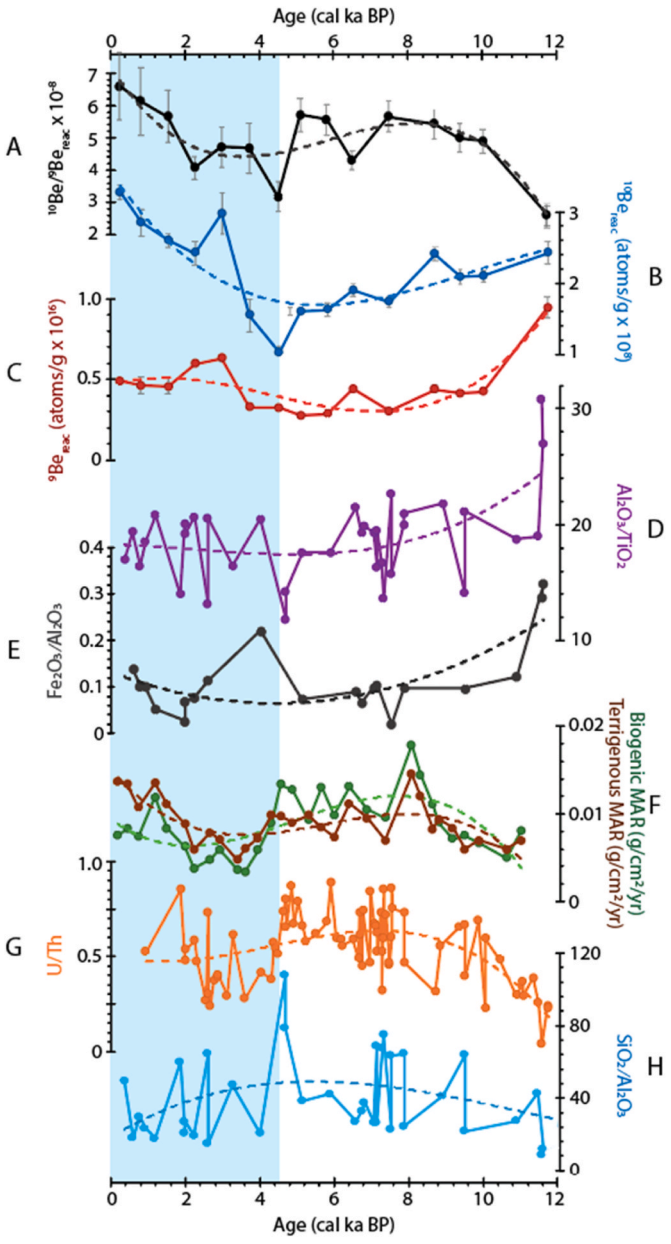

Fig. 2. Results from site U1357: A) $(^{10}Be/^{9}Be)_{reac}$ ratio; B) $^{10}Be_{reac}$ concentration; C) $^{9}Be_{reac}$ concentration; D) Al_2O_3/TiO_2, E) Fe_2O_3/Al_2O_3, F) biogenic MAR (g/cm^2/yr) and terrigenous MAR (g/cm^2/yr) (Ashley et al., 2021); G) U/Th; H) SiO_2/Al_2O_3. The shaded region denotes the late Holocene during which we see the greatest environmental changes and increases in $^{10}Be_{reac}$ and $(^{10}Be/^{9}Be)_{reac}$.

hydroxylamine hydrochloride ($NH_2OH.HCl$) in 25% acetic acid at 80 °C for 6 h (Bourles et al., 1989; Sproson et al., 2021a). Leaching for too long may attack the unwanted detrital phases of beryllium (the organic and residual phases) (Bourles et al., 1989; Sproson et al., 2021b). The leachate was dried down in hydrochloric acid (HCl), perchloric acid ($HClO_4$), and nitric acid (HNO_3), then diluted to 20 ml with MilliQ water. A 2 ml (10%) aliquot was taken for ^{9}Be analysis, and the remaining 90% of the leached sample was purified for ^{10}Be analysis via solvent extraction (Bourles et al., 1989) and precipitation cleaning (Sproson et al., 2021a). The ^{9}Be aliquot was dissolved in 10 ml of 5% HNO_3, then spiked with 1 ppm indium to correct for matrix effects before analysis by ELEMENT XR inductively coupled plasma mass spectrometry (ICP-MS) at the Atmosphere and Ocean Research Institute, The University of Tokyo (Sproson et al., 2021b). All values were

corrected according to their full chemistry procedural blanks. The oxidized ^{10}Be samples were pressed with pure niobium and analyzed by accelerator mass spectrometry at MALT (Micro Analysis Laboratory, Tandem Accelerator), The University of Tokyo (Yokoyama et al., 2019a; Matsuzaki et al., 2007). The KNB5-2 standard (^{10}Be/^{9}Be = 8.558 × 10^{-12}) was used to obtain absolute values (Nishiizumi et al., 2007). For a more in-depth description of analytical procedures, see Sproson et al. (2021b). We are using an updated age model proposed by Johnson et al. (2021) which adjusts the modern carbon contamination of the compound specific radiocarbon dating (Yamane et al., 2019) performed by Yamane et al. (2014). See Johnson et al. (2021) for a detailed description.

4. Results

The $^{9}Be_{reac}$ concentrations range from 2.81 ± 0.16 to 9.46 ± 0.68 × 10^{15} atoms g^{-1} with an average of 4.55 × 10^{15} atoms g^{-1}. The concentrations of $^{10}Be_{reac}$ range from 1.02 ± 0.1 to 2.98 ± 0.3 × 10^{8} atoms g^{-1} with an average of 2.09 × 10^{8} atoms g^{-1} (Fig. 2C, B, Table 1). The range of $(^{10}Be/^{9}Be)_{reac}$ is 2.56 ± 0.34 to 6.14 ± 1.06 x 10^{-8} with an average of 4.81 × 10^{-8} (Fig. 2A, Table 1).

After post-LGM grounded ice retreat, formation of a laminated sediment drift in the Adélie Basin commenced, preserving a record of Holocene glacimarine and hemipelagic processes (Expedition 318 Scientists, 2011; Ashley et al., 2021). Previously published shipboard x-ray fluorescence measurements from hole U1357A show there is a narrow range of variability of elemental concentrations in the Adélie Basin (Expedition 318 Scientists, 2011). High SiO_2 content (Fig. 3A) combined with the lithological classification of Unit I as diatom ooze (Fig. 4; 80–99% diatoms, Expedition 318 Scientists, 2011) indicates an abundance of siliceous diatoms. The relationship of SiO_2 vs. Al_2O_3 (Fig. 3A) display a negative correlation, and the higher values of Al_2O_3 correspond to samples at the bottom of the core, suggesting increased terrigenous content shortly after/during grounded ice retreat. The TiO_2 vs. Al_2O_3 and Fe_2O_3 vs. Al_2O_3 plots (Fig. 3B and C) display a positive correlation, suggesting these metals are from the same detrital source (Young and Nesbitt, 1998).

The highest Al_2O_3/TiO_2 and Fe_2O_3/Al_2O_3 ratios (Fig. 2D and E), used here as an indicator of change in sediment provenance, sorting, or degree of weathering (Young and Nesbitt, 1998), occur at the bottom of the core, suggesting that higher terrigenous input occurred at this time, concurrent with the retreat of proximal grounded ice. Excluding the bottommost sample, which has anomalously high values of $^{9}Be_{reac}$ and Al_2O_3/TiO_2, the $^{9}Be_{reac}$ is not correlated with the Al_2O_3/TiO_2 ratio after 10 ka BP ($R^2 = 0.16$, $p = .169$) suggesting $^{9}Be_{reac}$ was not sourced from local terrigenous export after this time. The $^{10}Be_{reac}$ values are positively correlated to $^{9}Be_{reac}$ ($R^2 = 0.39$, $p = .017$), and shows no correlation to the Al_2O_3/TiO_2 ratio, suggesting it has a similar source and mode of deposition as the $^{9}Be_{reac}$.

Biogenic and terrigenous mass accumulation rates (MARs) presented by Ashley et al. (2021) are correlated ($R^2 = 0.39$, $p < .001$) with highest values at ca. 8.2 ka BP, a decrease to lowest values from ca. 4.2 to 3.5 ka BP, followed by an increase from ca. 3.5 ka BP (Fig. 2E and F). The variations in biogenic and terrigenous MARs broadly covary with the $(^{10}Be/^{9}Be)_{reac}$ variations (Fig. 2). The U/Th ratio (Fig. 2G) can be used as an indicator of bottom water redox conditions (Kumar et al., 1995; Francois et al., 1997; Gallego-Torres et al., 2007). During the early through middle Holocene there is an overall increase in U/Th ratios, followed by a decrease at ca. 4.5 ka BP. Bottom water redox conditions may indicate variation in seasonal sea ice extent and duration, changes in ocean current intensity, and levels of productivity (Kumar et al., 1995; Francois et al., 1997; Gallego-Torres et al., 2007).

Table 1
Age, depth, and concentrations of $^{9}Be_{reac}$, $^{10}Be_{reac}$, and $(^{10}Be/^{9}Be)_{reac}$ for Adélie Basin hole U1357A. All samples are from Unit I (laminated diatom ooze) except for sample 20H1W-35_37 which is from Unit II (mud-rich diatom ooze).

Core ID: U1357A	Age (y)	Depth (m)	$^{9}Be_{reac}$ (10^{15} at g^{-1})	$^{10}Be_{reac}$ (10^{8} at g^{-1})	$(^{10}Be/^{9}Be)_{reac}$ (10^{-8})
1H1W-35_37	243	0.36	4.95 ± 0.64	3.27 ± 0.09	6.62 ± 1.06
2H1W-33_35	817	7.94	4.64 ± 0.50	2.85 ± 0.18	6.14 ± 1.06
3H1W-37_39	1539	17.48	4.59 ± 0.50	2.60 ± 0.10	5.66 ± 0.82
4H1W-35_37	2257	26.96	5.99 ± 0.14	2.42 ± 0.16	4.04 ± 0.36
6H1W-35_37	2984	45.96	6.35 ± 0.21	2.98 ± 0.30	4.69 ± 0.62
7H3W-35_37	3729	57.81	3.32 ± 0.08	1.54 ± 0.22	4.66 ± 0.79
8H3W-37_39	4515	66.84	3.27 ± 0.19	1.02 ± 0.10	3.12 ± 0.47
9H1W-35_37	5108	74.46	2.81 ± 0.16	1.60 ± 0.05	5.71 ± 0.52
10H1W-37_39	5817	83.98	2.92 ± 0.09	1.62 ± 0.10	5.56 ± 0.50
11H1W-34_36	6508	93.45	4.44 ± 0.12	1.90 ± 0.09	4.28 ± 0.31
15H2W-35_37	7481	132.07	3.06 ± 0.12	1.73 ± 0.08	5.66 ± 0.48
16H1W-36_38	8713	140.96	4.43 ± 0.21	2.41 ± 0.09	5.43 ± 0.47
17H1W-35_37	9392	150.46	4.19 ± 0.17	2.09 ± 0.10	4.99 ± 0.44
18H1W-40_42	10018	160.01	4.29 ± 0.16	2.10 ± 0.08	4.89 ± 0.37
20H1W-35_37	11742	178.96	9.46 ± 0.68	2.42 ± 0.15	2.56 ± 0.34

5. Discussion

5.1. Comparison of Antarctic beryllium isotope records

In this section we will compare our beryllium isotope data with that of previously published Adélie Basin ^{10}Be to assess differences caused by different extraction methods – leaching vs. whole rock decomposition (Fig. 4). We also compare to other sites from the Southern Ocean and Antarctica to see if the small, semi-enclosed and isolated Adélie Basin's $(^{10}Be/^{9}Be)_{reac}$ variations are similar to that of Antarctic lakes, sub-ice shelf/continental shelf, or an open marine environment (Fig. 1A, Table 2). Determining which environment the Adélie Basin is similar to may aid in assessing which mechanisms affect beryllium isotope variations in the Adélie Basin during the Holocene. We compare our data to lacustrine $(^{10}Be/^{9}Be)_{reac}$ (Lakes Skallen and Maruwan Oike; Sproson et al., 2021a), Ross Sea ^{10}Be/^{9}Be (Sjunneskog et al., 2007), Prydz Bay $(^{10}Be/^{9}Be)_{reac}$ (White et al., 2019), and the $(^{10}Be/^{9}Be)_{reac}$ of a nearby site offshore Wilkes Land (Valletta et al., 2018) excluding $^{10}Be_{reac}$ and $^{9}Be_{reac}$ of glacial diamict since the sediments analyzed here did not include diamict (Table 2).

The $^{9}Be_{reac}$ concentrations are lower than offshore Wilkes Land values of 16.9–27.2 × 10^{15} atoms g^{-1} but compare well with Lützow-Holm Bay lacustrine sediment values of 2.02–17.2 × 10^{15} atoms g^{-1} (Table 2). The Adélie Basin $^{10}Be_{reac}$ concentrations fall below those of both offshore Wilkes Land (1.3–12.7 × 10^{8} atoms g^{-1}) and Lützow-Holm Bay (0.5–13.6 × 10^{8} atoms g^{-1}) (Valletta et al., 2018; Sproson et al., 2021a). Compared to the previous results from the Adélie Basin, our $^{10}Be_{reac}$ concentrations are roughly half the whole rock ^{10}Be concentrations previously recorded (Table 2).

Based on the comparison of the two data sets from the Adélie Basin using the age model from Johnson et al. (2021), the discrepancy between the $^{10}Be_{reac}$ and previously measured whole rock ^{10}Be from the Adélie Basin (Behrens et al., 2019) appears to be due to different extraction methods (Fig. 4, Table 2). Behrens et al. (2019) used a whole rock decomposition method to isolate the ^{10}Be (Yokoyama et al.,

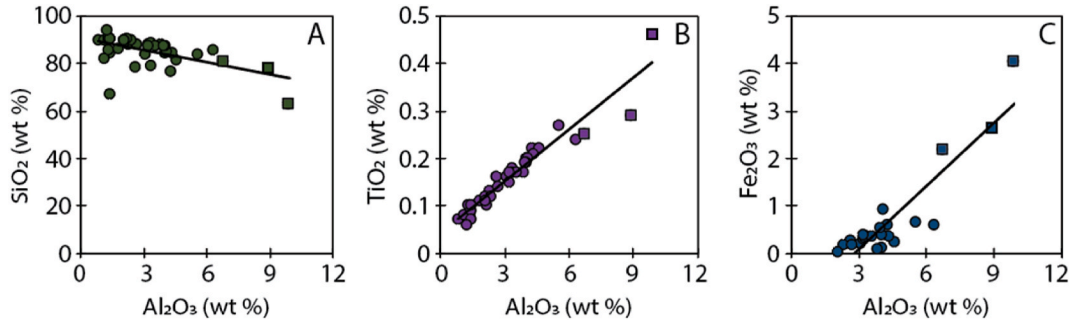

Fig. 3. Scatter plots of Adélie Basin A) SiO_2 vs. Al_2O_3; B) TiO_2 vs. Al_2O_3; C) Fe_2O_3 vs. Al_2O_3. The squares in each plot correspond to the same three bottom-most samples where the highest amount of terrigenous input was observed in the sediment core.

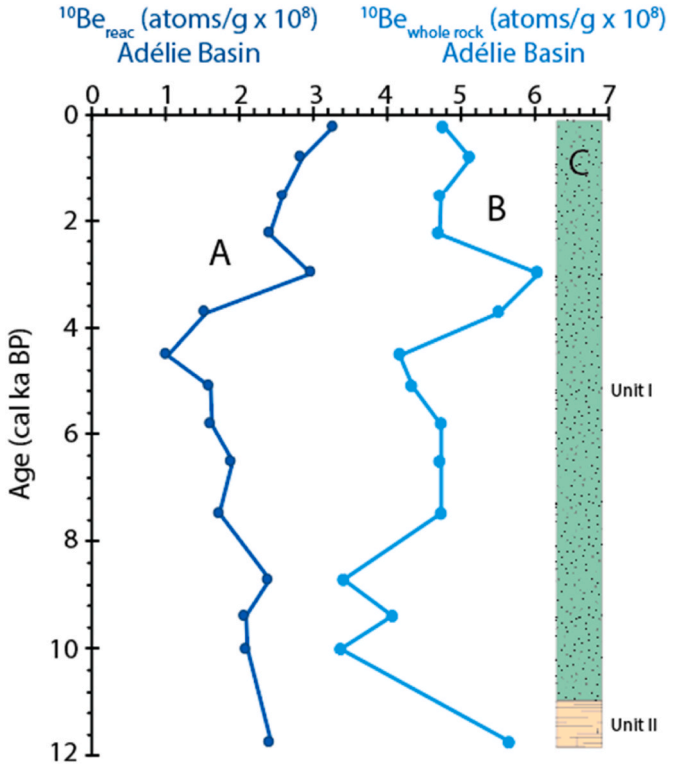

Fig. 4. Results of Adélie Basin $^{10}Be_{reac}$ from (A) this study, (B) whole rock ^{10}Be results from Behrens et al. (2019), and (C) lithology of hole U1357A.

2019a), collecting all phases, i.e., the exchangeable, calcium carbonate, Fe and Mn oxyhydroxide, organic matter, and detrital phases, from the sample (Tessier et al., 1979; Bourles et al., 1989). Here, we used a leaching agent to extract the $^{10}Be_{reac}$ representing the exchangeable, calcium carbonate, and Fe and Mn oxyhydroxide phases (Bourles et al., 1989; Sproson et al., 2021b), which can account for up to 70% of the ^{10}Be from the sample (Bourles et al., 1989; Wittmann et al., 2012). However, the $^{10}Be_{reac}$ values from this study are roughly half the ^{10}Be from the previous study (Fig. 4), suggesting the leach was more conservative, extracting ~50% of the ^{10}Be from the sample. The greatest discrepancy between the two records occurs at the bottom of the core from ca. 11.7 to 10 ka BP (Fig. 4). The lowermost sample of the whole rock ^{10}Be is much higher than the $^{10}Be_{reac}$, likely due to the influence of continental detritus released through basal erosion during the local phase of grounded ice retreat from the Adélie Basin (White et al., 2019; Ashley et al., 2021). The terrigenous debris from erosion may contain inherited meteoric ^{10}Be from accumulation of cosmogenic nuclides during the last warm period prior to glaciation (Graly et al., 2018). After ca. 8.5 ka BP, the two data sets show some agreement in variability,

Table 2
This study and previous studies' maximum and minimum values of $^{10}Be_{reac}$ and $^{9}Be_{reac}$, not including values from glacial diamict.

	Max $^{10}Be_{reac}$ (10^8 atoms g^{-1})	Min $^{10}Be_{reac}$ (10^8 atoms g^{-1})	Max $^{9}Be_{reac}$ (10^{15} atoms g^{-1})	Min $^{9}Be_{reac}$ (10^{15} atoms g^{-1})
This study (*Holocene, continental shelf*)	3.28 ± 0.10	0.78 ± 0.08	11.24 ± 0.23	1.25 ± 0.06
Sproson et al. (2021a) (*Holocene, lacustrine*)	13.64 ± 0.82	0.52 ± 0.20	17.18 ± 0.10	2.02 ± 0.01
[a]Behrens et al. (2019) (*Holocene, continental shelf*)	7.81 ± 1.51	2.31 ± 0.12	–	–
White et al. (2019) (*core top, open marine*)	9.86 ± 0.23	1.73 ± 0.05	~16.9	~7.9
White et al. (2019) (*core top, sub-ice shelf*)	11.1 ± 0.29	2.48 ± 0.06	~42.7	~18.1
Valletta et al. (2018) (*Pliocene, open marine*)	12.74 ± 0.17	1.29 ± 0.20	27.21 ± 1.54	16.90 ± 0.74
Sjunneskog et al. (2007) (*core top, continental shelf*)	17.7	0.28	–	–

[a] Note: Behrens et al. (2019) ^{10}Be values are not "reactive" but ^{10}Be from whole rock decomposition; this study did not analyze ^{9}Be.

decreasing to the lowest ^{10}Be concentrations in the core at ca. 4.5 ka BP (Fig. 4). From here, both records show an increase in ^{10}Be until 3 ka BP where there is a small decrease in values before another increase until the top of the core (Fig. 4). The largely similar trends, particularly after ca. 8.5 ka BP, suggest the whole rock ^{10}Be record from the Adélie Basin is valid, despite the possibility of having been affected by variables which do not reflect environmental forcing mechanisms, such as particle size (Wittmann et al., 2012; Simon et al., 2016).

Lakes Maruwan Oike and Skallen $^{10}Be_{reac}$ and $^{9}Be_{reac}$ from the Soya Coast (Sproson et al., 2021a) have similar values to the Adélie Basin marine samples, but the $^{10}Be_{reac}$ maximum values have higher concentrations than the Adélie Basin $^{10}Be_{reac}$ (Fig. 5, Table 2). Their sediment leach was 1 h longer than ours, meaning they may have leached up to 10% more $^{10}Be_{reac}$ and $^{9}Be_{reac}$ from the sediment samples (Simon et al., 2020). However, this is not enough to account for the difference in maximum values. A further explanation is that the lakes are closer to the glacial source and would have had a more restricted catchment area and higher concentration of beryllium isotopes. The $(^{10}Be/^{9}Be)_{reac}$ of both the lake records and the Adélie Basin record increase from ca. 4 ka BP and again from ca. 2.5 ka BP (Fig. 5), perhaps indicating similar timing of retreat and related mechanisms, such as increased terrigenous sedimentation and productivity, in both study sites. However, in this lake study, the Al_2O_3/TiO_3 and $^{9}Be_{reac}$ are correlated (Sproson et al., 2021a),

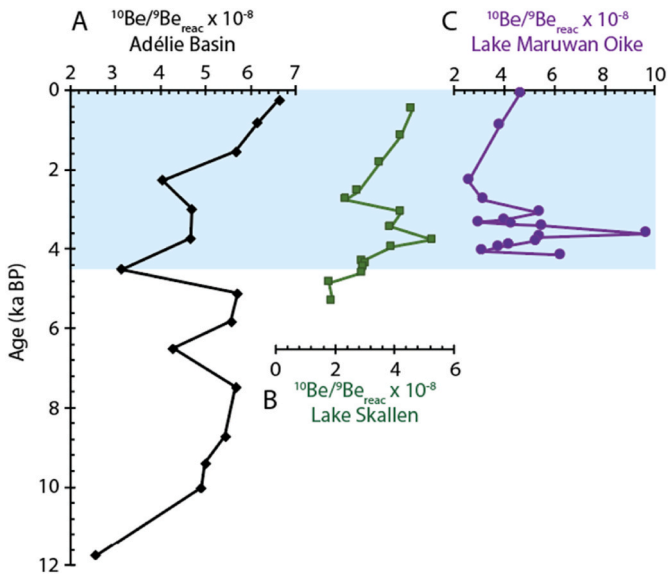

Fig. 5. Adélie Basin ($^{10}Be/^{9}Be)_{reac}$ (this study), Lake Skallen and Lake Maruwan Oike ($^{10}Be/^{9}Be)_{reac}$ (Sproson et al., 2021a). The shaded region denotes the late Holocene during which we see the greatest environmental changes and increases in $^{10}Be_{reac}$ and ($^{10}Be/^{9}Be)_{reac}$.

as opposed to our study (after 10 ka BP), suggesting a non-terrestrial source for $^{9}Be_{reac}$ in the Adélie Basin during the middle and late Holocene.

Data from Prydz Bay (White et al., 2019) and the Ross Sea (Sjunneskog et al., 2007) also show a greater range of values than the $^{10}Be_{reac}$ and $^{9}Be_{reac}$ from the Adélie Basin (Table 2). In these studies, core top sediment at varying distances from the coast was analyzed to assess the relationship between beryllium isotope concentrations and depositional environment. Prydz Bay ($^{10}Be/^{9}Be)_{reac}$ show higher values in open marine core tops than sub-ice shelf core tops (White et al., 2019), largely due to the higher contribution of $^{9}Be_{reac}$ in the sub-ice shelf environment (Table 2). Data from the Ross Sea shows increasing meteoric ^{10}Be with open water conditions (Sjunneskog et al., 2007). In a separate Ross Sea study, a change in sediment supply from deglaciation and concurrent increases in diatom productivity and meteoric ^{10}Be (Yokoyama et al., 2016), similar to the resemblance between ($^{10}Be/^{9}Be)_{reac}$ and biogenic and terrigenous MAR trends in the Adélie Basin (Fig. 2A, E), suggest there may be a relationship between increasing productivity and/or sediment supply and beryllium scavenging.

Wilkes Land Pliocene $^{10}Be_{reac}$ and $^{9}Be_{reac}$ (Valletta et al., 2018) have a greater range of values than the Adélie Basin, as expected (Table 2). As they were evaluating Be isotope variability across glacial-interglacial cycles, there would have been greater variability in maximum and minimum ice extent, hence greater variability in melting and basal erosion during the transition from glacial to interglacial conditions. Furthermore, they used a stronger leach, extracting a higher percentage of $^{10}Be_{reac}$ and $^{9}Be_{reac}$ from the samples (Bourles et al., 1989; Simon et al., 2020; Sproson et al., 2021b).

Considering the maximum and minimum values of both $^{10}Be_{reac}$ and $^{9}Be_{reac}$, the above comparisons demonstrate beryllium variations in the Adélie Basin most closely resemble that of the lake environment, though with lower maximum values (Table 2; Fig. 5). The lower maximum values may be due to its more exposed environment, open to influences such as ocean currents and changes in sea ice extent and primary productivity in addition to glacial advance and retreat, whereas lacustrine sediments are closer to the glacial source with restricted influence from oceanic mechanisms. The Adélie Basin $^{10}Be_{reac}$ and $^{9}Be_{reac}$ are also similar to those of Prydz Bay open marine core top $^{10}Be_{reac}$ and $^{9}Be_{reac}$ values (Table 2), which suggests the basin was not a sub-ice shelf environment during the Holocene.

5.2. The $^{10}Be_{reac}$ vs. $^{9}Be_{reac}$ relationship

The ($^{10}Be/^{9}Be)_{reac}$ is a more dependable proxy than ^{10}Be used without a normalizing isotope. The relationship between relative $^{10}Be_{reac}$ and $^{9}Be_{reac}$ can be interpreted as follows: (1) a 1:1 relationship (gray dotted line in Fig. 6) between the relative values signifies the ($^{10}Be/^{9}Be)_{reac}$ variability is largely controlled by extraction efficiency, scavenging rates, and/or dilution; (2) if the slope is less than one, additional variability in ($^{10}Be/^{9}Be)_{reac}$ reflects an additional input of $^{10}Be_{reac}$ (Von Blanckenburg et al., 2015), possibly due to variations in freshwater input (Simon et al., 2016; Valletta et al., 2018; Sproson et al., 2021a); and (3) a relationship greater than one is caused by additional $^{9}Be_{reac}$ input relative to $^{10}Be_{reac}$, possibly from additional weathering as discussed below. The relationship of relative $^{10}Be_{reac}$ vs. $^{9}Be_{reac}$ for different locations around East Antarctica at sites in the Adélie Basin (this study), Wilkes Land (Valletta et al., 2018), and Lakes Skallen and Maruwan Oike (Sproson et al., 2021a), are displayed in Fig. 6. Only Wilkes Land displays a slope less than one, from which we can infer additional $^{10}Be_{reac}$ variability relative to $^{9}Be_{reac}$ (Von Blanckenburg et al., 2015), possibly due to meltwater-derived $^{10}Be_{reac}$ input (Valletta et al., 2018).

The sample from the bottom of the sediment core measured here displays a >1:1 relationship suggesting additional ^{9}Be input when compared to the rest of the core (Fig. 6, red square), indicative of greater subglacial input during early Holocene grounding line retreat. Subsequently, the Adélie Basin relative $^{10}Be_{reac}$ vs. $^{9}Be_{reac}$ is very nearly in line with the 1:1 trendline ca. 10 ka BP, demonstrating glacial retreat was not the primary mechanism controlling $^{10}Be_{reac}$ and $^{9}Be_{reac}$ variations during the Holocene. Rather, the $^{10}Be_{reac}$ vs. $^{9}Be_{reac}$ were also controlled by changes in scavenging and/or dilution from the early Holocene. We have ruled out changes in extraction efficiency since all samples were consistently leached for 6 h, and there was no change in the strength of the leaching agent while performing the experiments.

The trend from the Wilkes Land beryllium data (Valletta et al., 2018) connects two main clusters (Fig. 6); these indicate the glacial periods when there was little $^{10}Be_{reac}$ transported offshore, and transition/interglacial periods when there was increased offshore transport of $^{10}Be_{reac}$ and $^{9}Be_{reac}$, interpreted to be sourced from meltwater and basal erosion, respectively, and delivered to the deep ocean via Antarctic Bottom Water (Valletta et al., 2018). Yet the high beryllium isotope

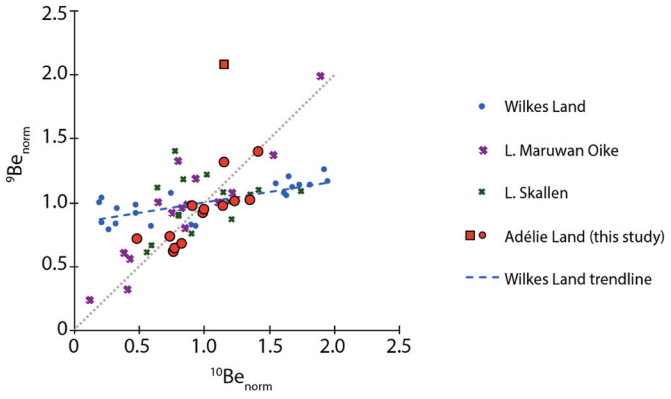

Fig. 6. Normalized $^{9}Be_{reac}$ vs. $^{10}Be_{reac}$ from this study (red symbols), Wilkes Land (blue circles, Valletta et al., 2018), and Lakes Skallen (green crosses) and Maruwan Oike (purple crosses), Lutzow-Holm Bay (Sproson et al., 2021a). The gray dotted line denotes a slope equal to one. A trendline less than one, for example, the Wilkes Land trendline (blue), suggests additional meteoric ^{10}Be was provided by glacial melt. The red square outlier represents the bottom-most sample of U1357A where the highest amount of ^{9}Be was measured, corresponding to high amounts of terrigenous input. (For interpretation of the references to colour in this figure legend, the reader is referred to the Web version of this article.)

concentrations occur during periods of high productivity, indicated by the opal and Ba/Al data in Valletta et al. (2018), suggesting higher beryllium concentration may be due to greater scavenging of available beryllium.

5.3. Holocene ice sheet dynamics inferred from $(^{10}Be/^{9}Be)_{reac}$

In the early Holocene, the $(^{10}Be/^{9}Be)_{reac}$ values increase sharply from ca. 11.5 to 10 ka BP corresponding with deglaciation from Terre Adélie continental shelf (Mackintosh et al., 2014) and decreasing $^{9}Be_{reac}$ (Fig. 2). Since $^{9}Be_{reac}$ is released to the reactive phase through weathering and leaves the weathering zone by erosion, high values of $^{9}Be_{reac}$ reflect periods of increased basal erosion (White et al., 2019; Sproson et al., 2021a). The highest $^{9}Be_{reac}$ value occurs at the bottom of the core (Fig. 2C) concurrent with the timing of proximal grounded ice retreat and a higher percentage of sand, silt, and clay in hole U1357A-Unit II, and the presence of ice rafted debris (Ashley et al., 2021, Fig. 4). Additionally, the Al_2O_3/TiO_3 ratio, an indicator of detrital input (Minyuk et al., 2014), is at its peak (Fig. 2D), and U/Th, an indicator of oxygenation (Kumar et al., 1995; Francois et al., 1997; Gallego-Torres et al., 2007), is at its lowest at the bottom of the core (Fig. 2G) indicating high detrital input and well oxygenated conditions (low U/Th) due to glacial retreat. Core MD03-2601, extracted from the continental shelf in this region (Fig. 1C), contains a record of Holocene glacial retreat following the LGM. Detrital proxies such as aluminum, thorium-232 content and lithic grain percentage from MD03-2601 show peaks in the early Holocene, supporting increased bedrock erosion due to glacier retreat (Denis et al., 2009). Furthermore, the TiO_2 vs. Al_2O_3 and Fe_2O_3 vs. Al_2O_3 relationships show no change in sediment source (Young and Nesbitt, 1998, Fig. 3B and C).

Between 11.4 and 8.5 ka BP, the U-shaped bathymetric trough of the Adélie Basin is interpreted to have been characterized by a calving bay re-entrant glacial system, whereby seasonally open water existed in the trough, but ice was still grounded on the shallower banks around the Adélie Basin (Leventer et al., 2006; Expedition 318 Scientists, 2011, Fig. 7). By ca. 8 ka BP, sedimentary data suggests most of this residual ice sheet had disappeared due to melt, connecting the Adélie Basin to the Adélie Depression via a small chasm along the Adélie Bank and opening the basin to advection of particles via the ACC. This is supported by increases in biogenic and terrigenous MARs at 8 ka BP (Ashley et al., 2021, Fig. 2E and F).

The uniform $(^{10}Be/^{9}Be)_{reac}$ from ca. 8.5 to 5 ka BP indicates stable conditions during the middle Holocene (Fig. 2A, Table 1). There is less input of sand and ice rafted debris, suggesting local terrigenous sediment supply is restricted (Ashley et al., 2021; Johnson et al., 2021), while $^{10}Be_{reac}$ decreases until ca. 4.5 ka BP to its lowest concentration in the core of $1.02 \pm 0.1 \times 10^{8}$ atoms g^{-1} (Fig. 2B, Table 1). The $^{9}Be_{reac}$ remains consistently low until ca. 3.7 ka BP, decreasing to $3.32 \pm 0.08 \times 10^{15}$ atoms g^{-1} (Fig. 2C, Table 1). Detrital proxies from hole MD03-2601 in the Dumont D'Urville Trough also show a general decreasing trend in terrigenous supply until 4.5 ka BP (Denis et al., 2009; Ashley et al., 2021), and low variation in *Chaetoceros* resting spore (CRS) abundance in MD03-2601 suggests limited water stratification and decreased melt rates/basal erosion due to limited glacial activity (Denis et al., 2009). Since glacial activity was limited from ca. 8.5 to 4.5 ka BP, it is likely another mechanism was responsible for the small variations in the beryllium isotopes during this time.

Similarity between the $(^{10}Be/^{9}Be)_{reac}$ and biogenic and terrigenous MAR trends (Fig. 2) suggest productivity and scavenging may be related to variations in $^{10}Be_{reac}$ and $^{9}Be_{reac}$ from ca. 8.5 ka BP (Fig. 7). The U/Th values were higher during the middle Holocene (Fig. 2G), indicating increased productivity and an increased supply of organic matter (Kumar et al., 1995; Francois et al., 1997; Gallego-Torres et al., 2007). However, the biogenic and terrigenous MARs are not solely a function of productivity but also represent an indication of current strength and sediment advection to the site (Johnson et al., 2021), including the increase of $^{10}Be_{reac}$ and $^{9}Be_{reac}$ at ca. 8 ka BP (Fig. 2B and C) corresponding to the start of particle advection via the ACC into the Adélie Basin (Fig. 7) and subsequent increases in biogenic and terrigenous MARs (Fig. 2; Ashley et al., 2021). During the middle Holocene from ca. 8 to 4.5 ka BP, the biogenic and terrigenous MARs are relatively high (Fig. 2F), indicating a stronger ACC and reduced influence of coastal sea ice coverage (Johnson et al., 2021). The advection of particles to the Adélie Basin would have supplied additional particles for the scavenging of $^{10}Be_{reac}$ and $^{9}Be_{reac}$ (Fig. 7). Furthermore, the $^{9}Be_{reac}$ vs. $^{10}Be_{reac}$ relationship is 1:1 indicating scavenging/dilution are primary processes acting on $(^{10}Be/^{9}Be)_{reac}$ during this time, rather than glacial processes affecting $^{10}Be_{reac}$ or $^{9}Be_{reac}$ (Fig. 6).

Environmental conditions began to cool in the late Holocene (from 4.5 ka BP), as indicated by an increase in *F.curta* sea ice diatom percent from core MD03-2601 (Renssen et al., 2005; Crosta et al., 2007; Denis et al., 2009), and Adélie Basin beryllium isotopes are at their lowest values (Fig. 2, Table 1) corresponding to the sudden increase in coastal sea ice observed in diatom and organic biomarker proxies (Crosta et al., 2018; Ashley et al., 2021; Johnson et al., 2021). However, both $(^{10}Be/^{9}Be)_{reac}$ and $^{10}Be_{reac}$ begin to increase from ca. 4.5 to 3 ka BP and again from ca. 2.2 ka BP, and $^{9}Be_{reac}$ values increase as well at ca. 3.7 ka BP before decreasing again (Fig. 2). One possible explanation for increasing $(^{10}Be/^{9}Be)_{reac}$ during the late Holocene may be that the greater sea ice extent acted as an insulator, allowing subsurface water temperatures to increase due to enhanced Southern Ocean stratification (Crosta et al., 2007, Crosta et al., 2018; Silvano et al., 2018; Sadai et al., 2020). Basal melting due to warmer subsurface water may have contributed to the increase in beryllium isotopes during this period. However, occurrences of high terrigenous input at site MD03-2601 along with lower CRS abundances suggest episodes of ice advance were more probable than retreat (Denis et al., 2009).

Another explanation for increasing beryllium isotope values from 4.5 ka BP is that ice retreat in another location rather than local retreat influenced beryllium concentrations in the Adélie Basin. A decrease in ice core $\delta^{18}O$ around Antarctica (Masson et al., 2000) and warmer subsurface water corresponds to the thinning of several ice shelves around the continent, including the Ross Sea Ice Shelf (Yokoyama et al., 2016; Ashley et al., 2021). Beryllium isotope records from the Ross Sea show ice retreat and meltwater influx during the middle to late Holocene, corresponding to ongoing retreat of grounded ice sheet systems in the Ross Sea which peaked at ca. 4 ka BP (Yokoyama et al., 2019b) and development of the large modern Ross Ice Shelf cavity (Yokoyama et al., 2016; Mckay et al., 2016). The Adélie Basin lies along the path of the ACC which flows past the Ross Sea as it circulates west around the continent. Compound specific deuterium isotopes at the Adélie Basin Site U1357 have been interpreted to suggest meltwater input sourced from the Ross Sea peaked at ca. 4.5 ka BP before gradually decreasing and stabilizing by ca. 3 ka BP (Ashley et al., 2021). The increase in $(^{10}Be/^{9}Be)_{reac}$ (Fig. 2A) may be indirectly due to supercooled water masses that circulate beneath the Ross Ice Shelf and are subsequently advected into the Adélie Land region (Ashley et al., 2021). However, as above, the 1:1 relationship between $^{10}Be_{reac}$ vs. $^{9}Be_{reac}$ indicates scavenging efficiency has more of an effect on $(^{10}Be/^{9}Be)_{reac}$ variation during the late Holocene, as opposed to glacial processes (Fig. 6).

A third possibility is that $^{10}Be_{reac}$ and $^{9}Be_{reac}$ variations are a function of scavenging efficiency and dilution, as indicated by the $^{10}Be_{reac}$ vs. $^{9}Be_{reac}$ relationship (Fig. 6), as well as biogenic and terrigenous MARs (Fig. 2F). Though meltwater input sourced from the Ross Sea may not have contributed to beryllium variations in the Adélie Basin, these supercooled waters from the Ross Sea are proposed to have triggered increased coastal sea ice coverage from ca. 4.5 ka BP (Ashley et al., 2021; Crosta et al., 2018). Enhanced coastal sea ice and longer seasonal sea ice duration could have led to a background decrease in current strength and accumulation in the Adélie Basin (Johnson et al., 2021), supported by low biogenic and terrigenous MARs from ca. 4.5 to 2.2 ka BP (Fig. 2F). The relatively low $(^{10}Be/^{9}Be)_{reac}$ values from ca. 4.5 to 2.2

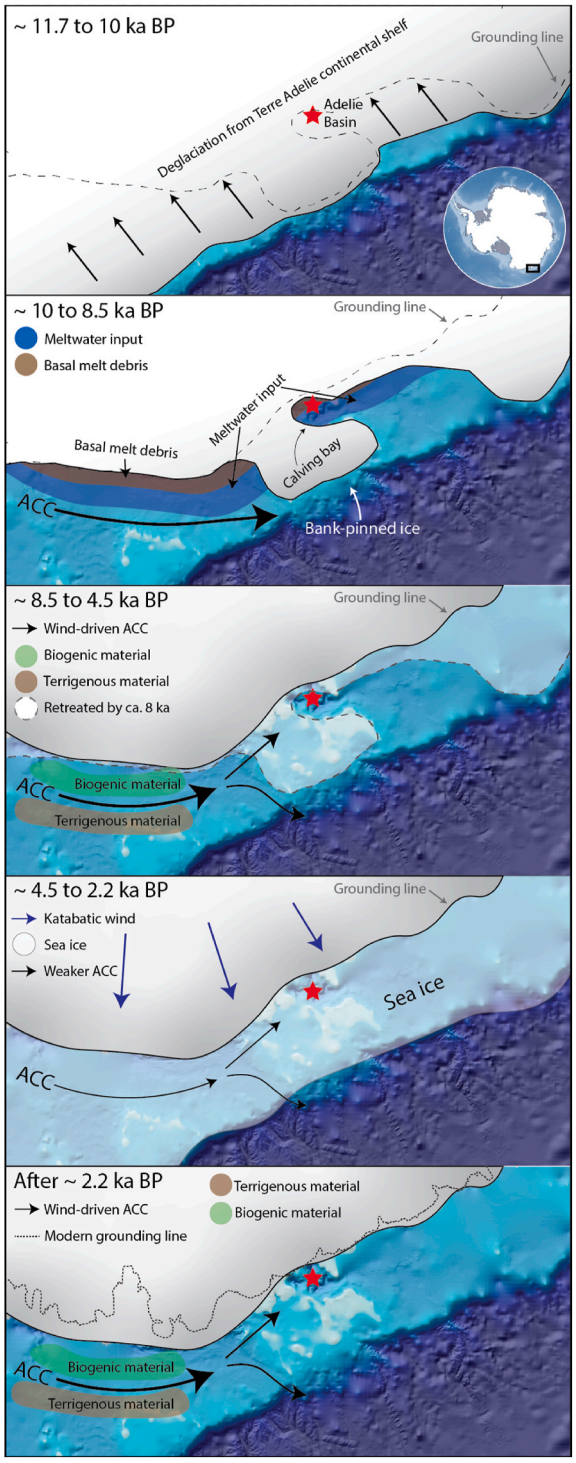

(caption on next column)

Fig. 7. Schematic of mechanisms affecting Be variations in the Adélie Basin. From ca. 11.7 to 10 ka BP: Deglaciation from the continental shelf and formation of U-shaped calving bay. Detrital input and meltwater from glacial retreat are main factors affecting variations of $^{9}Be_{reac}$ and $^{10}Be_{reac}$, respectively. From ca. 10 to 8.5 ka BP: $^{10}Be_{reac}$ variations largely affected by meltwater input from ice sheet retreat and icebergs; $^{9}Be_{reac}$ variations were caused by terrigenous debris from basal melt and ice rafted debris. From ca. 8.5 to 4.5 ka BP: the residual ice on the Adélie Bank retreats by ca. 8 ka BP allowing the wind-driven ACC to connect the Adélie Basin to the Adélie Depression. Increased influence from the Ross Sea via the ACC results in increasing biogenic and terrigenous MARs. Limited glacial activity suggests biogenic and terrigenous material advected by the ACC may be a factor in Be isotope variations. From ca. 4.5 to 2.2 ka BP increased sea ice coverage results in weaker ACC, decreased biogenic and terrigenous MARs, and lower Be isotope values. From ca. 2.2 ka BP, increasing biogenic and terrigenous MARs indicate stronger ACC and reduced seasonal sea ice extent. The $^{10}Be_{reac}$ and $^{9}Be_{reac}$ is scavenged by particles advected by the ACC and transported to the Adélie Basin. Base map bathymetry is from the IBCSO elevation model (Arndt et al., 2013). Early Holocene grounding line is based on Mackintosh et al. (2014) model output, and modern groundling line is from the MEaSUREs Antarctic Boundaries program (Rignot et al., 2013; Mouginot et al., 2017).

ka BP (Fig. 2A) may also reflect decreased productivity and particle availability due to the sudden intensification of coastal sea ice from ca. 4.5 ka BP. Advection of biogenic and terrigenous particles via the ACC would have been hindered until current speed increased again from ca. 2.2 ka BP, as indicated by increasing biogenic and terrigenous MARs (Johnson et al., 2021, Fig. 2). Increases in both biogenic/terrigenous MARs from 2.2 ka BP suggest a stronger current passing through to the Adélie Basin and an increase in $^{10}Be_{reac}$ and $^{9}Be_{reac}$ scavenging particles (Fig. 7). The greater increase in $^{10}Be_{reac}$ and relatively lower $^{9}Be_{reac}$ from ca. 2.2 ka BP (Fig. 2B and C), resulting in increasing $(^{10}Be/^{9}Be)_{reac}$ (Fig. 2A), may signify additional meteoric ^{10}Be input from episodes of melting sea ice (Frank et al., 2009).

5.4. Synthesis

During the early Holocene, from ca. 11.7 to 10 ka BP, deglaciation from the continental shelf and formation of a U-shaped calving bay, from which icebergs break off, seem to be the main mechanisms affecting $^{10}Be_{reac}$ and $^{9}Be_{reac}$ in the Adélie Basin through meltwater and basal erosion, respectively (Fig. 7). After 10 ka BP, the mechanisms affecting beryllium isotopes shift from glacially-driven variations to current-driven variations. Comparisons to lake, continental shelf, and open ocean beryllium isotope records from around Antarctica demonstrate the Adélie Basin beryllium isotope variations are similar to that of a lacustrine setting, though with smaller maximum values due to its more open environment and larger (diluted) catchment. This allows the ACC to influence beryllium isotope variations in the basin through changes in current strength and particle advection. The correlation between the Adélie Basin biogenic and terrigenous MARs with beryllium isotopes may indicate beryllium isotope concentrations also vary due to changes in current strength and particle advection (Bahr et al., 2014; Rebesco et al., 2014). Particularly for the middle and late Holocene, changes in glacial melt and basal erosion seem to have less of an effect, as indicated by the $^{10}Be_{reac}$ vs. $^{9}Be_{reac}$ relationship (Fig. 6). By ca. 8 ka BP, the residual ice on the Adélie Bank retreats, allowing the wind-driven ACC to influence the Adélie Basin resulting in increasing biogenic and terrigenous MARs (Fig. 7). Limited glacial activity in the middle and late Holocene and the $^{9}Be_{reac}$ vs. $^{10}Be_{reac}$ relationship suggests biogenic and terrigenous material advected by the ACC may lead to variations in beryllium isotopes. From ca. 4.5 to 2.2 ka BP increased sea ice coverage results in weaker ACC, decreased biogenic and terrigenous MARs, and lower beryllium isotope values (Figs. 2 and 7). From ca. 2.2 ka BP, increasing biogenic and terrigenous MARs indicate stronger ACC and reduced seasonal sea ice extent allowing for increased scavenging and deposition of $^{10}Be_{reac}$ and $^{9}Be_{reac}$ in the Adélie Basin (Fig. 7).

6. Conclusion

In a previously published study of ^{10}Be from the Adélie Basin, meltwater and glacial retreat is postulated as the main mechanism for variations in ^{10}Be during the Holocene. Our $(^{10}Be/^{9}Be)_{reac}$ data also indicate increased subglacial discharge immediately following grounded ice retreat at ca. 11.7 ka BP from the Adélie Basin continental shelf until ca. 10 ka BP. However, our data demonstrate glacial retreat, meltwater, and basal erosion are not solely responsible for variations in $^{10}Be_{reac}$, $^{9}Be_{reac}$, and $(^{10}Be/^{9}Be)_{reac}$ following this episode of grounded ice retreat, after ca. 10 ka BP. Changes in the strength of the ACC, which passes through the Ross Sea, are suggested to be largely responsible for changes in biogenic and terrigenous MARs in the Adélie Basin. The similarity between Adélie Basin biogenic and terrigenous MARs and the $(^{10}Be/^{9}Be)_{reac}$ curve suggest changes in availability of scavenging particles, controlled by biological productivity, and accumulation rate, dependent upon current strength, are significant additional controls on $^{10}Be_{reac}$ and $^{9}Be_{reac}$ variations which need to be considered in future studies in addition to glacial dynamics.

Overall, the current $(^{10}Be/^{9}Be)_{reac}$ data set from the Adélie Basin is controlled by scavenging efficiency and the influence of the high $^{9}Be_{reac}$ at the bottom of the core, but with a higher resolution data set and integration with a broad multiproxy dataset, it may be possible to better constrain the influence of climatic, cryosphere, and oceanographic mechanisms on beryllium isotopes throughout the Holocene. Though we have improved upon the Adélie Basin whole rock ^{10}Be record with $(^{10}Be/^{9}Be)_{reac}$ ratios, higher resolution records of $(^{10}Be/^{9}Be)_{reac}$ from the Southern Ocean would improve estimates of the timing of LGM ice retreat and variations in other processes which may affect the $(^{10}Be/^{9}Be)_{reac}$ of sediments.

Declaration of competing interest

The authors declare that they have no known competing financial interests or personal relationships that could have appeared to influence the work reported in this paper.

Acknowledgements

The authors would like to extend their sincere gratitude to H. Matsuzaki for support using the tandem accelerator mass spectrometer and T. Aze for overseeing the inductively coupled plasma mass spectrometry analyses. Special thanks to two anonymous reviewers for their insight and constructive comments which have helped to improve the manuscript. Financial support for this study was provided by the Japan Society for the Promotion of Science (JSPS) KAKENHI (20H00193) to YY, JSPS Fellowship DC1 (20J21145) to BCB, and JSPS Post-Doctoral Fellowship (PE17712 and P18791) to ADS. RM was funded by the New Zealand Ministry of Business, Innovation and Employment through the Antarctic Science Platform (ANTA1801). CE and FJJ-E acknowledges funding through Spanish Ministry of Science and Innovation (grant CTM2017-89711-C2-1-P), co-funded by the European Union through FEDER funds.

References

Arndt, J.E., Schenke, H.W., Jakobsson, M., Nitsche, F.O., Buys, G., Goleby, B., Rebesco, M., Bohoyo, F., Hong, J., Black, J., Greku, R., Udintsev, G., Barrios, F., Reynoso-Peralta, W., Taisei, M., Wigley, R., 2013. The International Bathymetric Chart of the Southern Ocean (IBCSO) Version 1.0 – a new bathymetric compilation covering circum-Antarctic waters. Geophys. Res. Lett. 40, 3111–3117.

Ashley, K.E., Mckay, R., Etourneau, J., Jimenez-Espejo, F.J., Condron, A., Albot, A., Crosta, X., Riesselman, C., Seki, O., Massé, G., 2021. Mid-Holocene Antarctic sea-ice increase driven by marine ice sheet retreat. Clim. Past 17, 1–19.

Bahr, A., Jiménez-Espejo, F.J., Kolasinac, N., Grunert, P., Hernández-Molina, F.J., Röhl, U., Voelker, A.H., Escutia, C., Stow, D.A., Hodell, D., Alvarez-Zarikian, C.A., 2014. Deciphering bottom current velocity and paleoclimate signals from contourite deposits in the G ulf of C ádiz during the last 140 kyr: an inorganic geochemical approach. G-cubed 15 (8), 3145–3160.

Baumhoer, C.A., Dietz, A.J., Kneisel, C., Paeth, H., Kuenzer, C., 2021. Environmental drivers of circum-Antarctic glacier and ice shelf front retreat over the last two decades. Cryosphere 15, 2357–2381.

Behrens, B., Miyairi, Y., Sproson, A.D., Yamane, M., Yokoyama, Y., 2019. Meltwater discharge during the Holocene from the Wilkes subglacial basin revealed by beryllium isotope analysis of marine sediments. J. Quat. Sci. 34, 603–608.

Bentley, M.J., Fogwill, C.J., Kubik, P.W., Sugden, D.E., 2006. Geomorphological evidence and cosmogenic 10Be/26Al exposure ages for the last glacial maximum and deglaciation of the Antarctic Peninsula ice sheet. Geol. Soc. Am. Bull. 118, 1149–1159.

Bourles, D., Raisbeck, G., Yiou, F., 1989. 10Be and 9Be in marine sediments and their potential for dating. Geochem. Cosmochim. Acta 53, 443–452.

Campagne, P., Crosta, X., Houssais, M.N., Swingedouw, D., Schmidt, S., Martin, A., Devred, E., Capo, S., Marieu, V., Closset, I., Massé, G., 2015. Glacial ice and atmospheric forcing on the Mertz Glacier Polynya over the past 250 years. Nat. Commun. 6, 6642.

Crosta, X., Debret, M., Denis, D., Courty, M.A., Ther, O., 2007. Holocene long- and short-term climate changes off Adélie Land, East Antarctica. G-cubed 8.

Crosta, X., Crespin, J., Swingedouw, D., Marti, O., Masson-Delmotte, V., Etourneau, J., Goosse, H., Braconnot, P., Yam, R., Brailovski, I., Shemesh, A., 2018. Ocean as the Main Driver of Antarctic Ice Sheet Retreat during the Holocene.

Denis, D., Crosta, X., Schmidt, S., Carson, D.S., Ganeshram, R.S., Renssen, H., Bout-Roumazeilles, V., Zaragosi, S., Martin, B., Cremer, M., 2009. Holocene glacier and deep water dynamics, Adélie Land region, East Antarctica. Quat. Sci. Rev. 28, 1291–1303.

Expedition 318 Scientists, 2011. Expedition 318 summary. In: Escutia, C., Brinkhuis, H., Klaus, A. (Eds.), The Expedition 318 Scientists, Proc. IODP. Integrated Ocean Drilling Program Management International, Inc.), Tokyo, 318.

Fogwill, C., Turney, C., Golledge, N., Etheridge, D., Rubino, M., Thornton, D., Baker, A., Woodward, J., Winter, K., Van Ommen, T., 2017. Antarctic ice sheet discharge driven by atmosphere-ocean feedbacks at the Last Glacial Termination. Sci. Rep. 7, 1–10.

Francois, R., Altabet, M.A., Yu, E.F., Sigman, D.M., Bacon, M.P., Frank, M., Bohrmann, G., Bareille, G., Labeyrie, L.D., 1997. Contribution of Southern Ocean surface-water stratification to low atmospheric CO 2 concentrations during the last glacial period. Nature 389 (6654), 929–935.

Frank, M., Porcelli, D., Andersson, P., Baskaran, M., Bjork, G., Kubik, P.W., Hattendorf, B., Guenther, D., 2009. The dissolved Beryllium isotope composition of the Arctic Ocean. Geochimica et Cosmochimica Acta 73 (20), 6114–6133.

Fretwell, P., Pritchard, H.D., Vaughan, D.G., Bamber, J.L., Barrand, N., Bell, R., Bianchi, C., Bingham, R., Blankenship, D.D., Casassa, G., 2013. Bedmap2: Improved Ice Bed, Surface and Thickness Datasets for Antarctica.

Gallego-Torres, D., Martínez-Ruiz, F., Paytan, A., Jiménez-Espejo, F.J., Ortega-Huertas, M., 2007. Pliocene–Holocene evolution of depositional conditions in the eastern Mediterranean: role of anoxia vs. productivity at time of sapropel deposition. Palaeogeogr. Palaeoclimatol. Palaeoecol. 246 (2–4), 424–439.

Gille, S.T., 2008. Decadal-scale temperature trends in the Southern Hemisphere ocean. J. Clim. 21, 4749–4765.

Golledge, N.R., Fogwill, C.J., Mackintosh, A.N., Buckley, K.M., 2012. Dynamics of the last glacial maximum Antarctic ice-sheet and its response to ocean forcing. Proc. Natl. Acad. Sci. Unit. States Am. 109 (40), 16052–16056.

Golledge, N.R., Keller, E.D., Gomez, N., Naughten, K.A., Bernales, J., Trusel, L.D., Edwards, T.L., 2019. Global environmental consequences of twenty-first-century ice-sheet melt. Nature 566 (7742), 65–72.

Graly, J.A., Corbett, L.B., Bierman, P.R., Lini, A., Neumann, T.A., 2018. Meteoric 10Be as a tracer of subglacial processes and interglacial surface exposure in Greenland. Quat. Sci. Rev. 191, 118–131.

Hay, C.C., Morrow, E., Kopp, R.E., Mitrovica, J.X., 2015. Probabilistic reanalysis of twentieth-century sea-level rise. Nature 517, 481–484.

Johnson, K.M., Mckay, R.M., Etourneau, J., Jiménez-Espejo, F.J., Albot, Riesselman, C. R., Bertler, N.A.N., Horgan, H.J., Crosta, X., Bendle, J., Ashley, K.E., Yamane, M., Yokoyama, Y., Pekar, S.F., Escutia, C., Dunbar, R.B., 2021. Sensitivity of Holocene East Antarctic productivity to subdecadal variability set by sea ice. Nat. Geosci. 14.

Jones, R.S., Norton, K.P., Mackintosh, A.N., Anderson, J.T.H., Kubik, P., Vockenhuber, C., Wittmann, H., Fink, D., Wilson, G.S., Golledge, N.R., Mckay, R., 2017. Cosmogenic nuclides constrain surface fluctuations of an East Antarctic outlet glacier since the Pliocene. Earth Planet Sci. Lett. 480, 75–86.

Kemppinen, K.M.S., Holden, P.B., Edwards, N.R., Ridgwell, A., Friend, A.D., 2018. Coupled climate-carbon cycle simulation of the Last Glacial Maximum atmospheric CO2 decrease using a large ensemble of modern plausible parameter sets. Clim. Past Discuss 2018, 1–52.

Kumar, N., Anderson, R.F., Mortlock, R.A., Froelich, P.N., Kubik, P., Dittrich-Hannen, B., Suter, M., 1995. Increased biological productivity and export production in the glacial Southern Ocean. Nature 378 (6558), 675–680.

Leventer, A., Domack, E., Pike, J., Stickley, C., Maddison, E., Brachfeld, S.A., Manley, P., Mcclennen, C., 2006. Marine Sediment Record from the East Antarctic Margin Reveals Dynamics of Ice Sheet Recession.

Mackintosh, A.N., Verleyen, E., O'brien, P.E., White, D.A., Jones, R.S., Mckay, R., Dunbar, R., Gore, D.B., Fink, D., Post, A.L., Miura, H., 2014. Retreat history of the East Antarctic ice sheet since the last glacial maximum. Quat. Sci. Rev. 100, 10–30.

Masson, V., Vimeux, F., Jouzel, J., Morgan, V., Delmotte, M., Ciais, P., Hammer, C., Johnsen, S., Lipenkov, V.Y., Mosley-Thompson, E., 2000. Holocene climate variability in Antarctica based on 11 ice-core isotopic records. Quat. Res. 54, 348–358.

Matsuzaki, H., Nakano, C., Tsuchiya, Y.S., Kato, K., Maejima, Y., Miyairi, Y., Wakasa, S., Aze, T., 2007. Multi-nuclide AMS performances at MALT. Nucl. Instrum. Methods Phys. Res. Sect. B Beam Interact. Mater. Atoms 259, 36–40.
Mckay, R., Golledge, N.R., Maas, S., Naish, T., Levy, R., Dunbar, G., Kuhn, G., 2016. Antarctic marine ice-sheet retreat in the Ross Sea during the early Holocene. Geology 44 (1), 7–10.
Mengel, M., Levermann, A., 2014. Ice plug prevents irreversible discharge from East Antarctica. Nat. Clim. Change 4, 451–455.
Miles, B.W., Stokes, C.R., Jamieson, S.S., 2016. Pan–ice-sheet glacier terminus change in East Antarctica reveals sensitivity of Wilkes Land to sea-ice changes. Sci. Adv. 2, e1501350.
Miles, B.W., Stokes, C.R., Jamieson, S.S., 2018. Velocity increases at Cook Glacier, East Antarctica, linked to ice shelf loss and a subglacial flood event. Cryosphere 12 (10), 3123–3136.
Minyuk, P., Borkhodoev, V.Y., Wennrich, V., 2014. Inorganic geochemistry data from Lake El'gygytgyn sediments: marine isotope stages 6–11. Clim. Past 10, 467–485.
Morlighem, M., Rignot, E., Binder, T., Blankenship, D., Drews, R., Eagles, G., Eisen, O., Ferraccioli, F., Forsberg, R., Fretwell, P., 2020. Deep glacial troughs and stabilizing ridges unveiled beneath the margins of the Antarctic ice sheet. Nat. Geosci. 13, 132–137.
Mouginot, J., Scheuchl, B., Rignot, E., 2017. MEaSUREs Antarctic Boundaries for IPY 2007-2009 from Satellite Radar, Version 2. [Grounding Line]. NASA National Snow and Ice Data Center Distributed Active Archive Center, Boulder, Colorado USA. https://doi.org/10.5067/AXE4121732AD.
Nishiizumi, K., Imamura, M., Caffee, M.W., Southon, J.R., Finkel, R.C., Mcaninch, J., 2007. Absolute calibration of 10Be AMS standards. Nucl. Instrum. Methods Phys. Res. Sect. B Beam Interact. Mater. Atoms 258, 403–413.
Pedro, J., Smith, A., Simon, K., Van Ommen, T., Curran, M., 2011. High-resolution records of the beryllium-10 solar activity proxy in ice from Law Dome, East Antarctica: measurement, reproducibility and principal trends. Clim. Past 7, 707–721.
Rebesco, M., Hernández-Molina, F.J., Van Rooif, D., Wåhlin, A., 2014. Contourites and associated sediments controlled by deep-water circulation processes: state-of-the-art and future considerations. Mar. Geol. 352, 111–154.
Renssen, H., Goosse, H., Fichefet, T., Masson-Delmotte, V., Koç, N., 2005. Holocene climate evolution in the high-latitude Southern Hemisphere simulated by a coupled atmosphere-sea ice-ocean-vegetation model. Holocene 15, 951–964.
Rignot, E., Jacobs, S.S., Mouginot, J., Scheuchl, B., 2013. Ice-shelf melting around Antarctica. Science 341, 266–270. https://doi.org/10.1126/science.1235798.
Sadai, S., Condron, A., Deconto, R., Pollard, D., 2020. Future climate response to Antarctic Ice Sheet melt caused by anthropogenic warming. Sci. Adv. 6, eaaz1169.
SCAR, 1992. Composite gazetteer of Antarctica (updated 2015) URL. http://gcmd.nasa.gov/records/SCAR_Gazetteer.html.
Scherer, R.P., Aldahan, A., Tulaczyk, S., Possnert, G., Engelhardt, H., Kamb, B., 1998. Pleistocene collapse of the west Antarctic ice sheet. Science 281, 82–85.
Silvano, A., Rintoul, S.R., Peña-Molino, B., Hobbs, W.R., Van Wijk, E., Aoki, S., Tamura, T., Williams, G.D., 2018. Freshening by glacial meltwater enhances melting of ice shelves and reduces formation of Antarctic Bottom Water. Sci. Adv. 4, eaap9467.
Simon, Q., Thouveny, N., Bourles, D.L., Nuttin, L., Hillaire-Marcel, C., St-Onge, G., 2016. Authigenic $^{10}Be/^{9}Be$ ratios and ^{10}Be-fluxes ($^{230}Th_{xs}$-normalized) in central Baffin Bay sediments during the last glacial cycle: paleoenvironmental implications. Quat. Sci. Rev. 140, 142–162.
Simon, Q., Thouveny, N., Bourlès, D.L., Valet, J.-P., Bassinot, F., 2020. Cosmogenic ^{10}Be production records reveal dynamics of geomagnetic dipole moment (GDM) over the Laschamp excursion (20–60 ka). Earth Planet Sci. Lett. 550, 116547.
Sjunneskog, C., Scherer, R., Aldahan, A., Possnert, G., 2007. ^{10}Be in glacial marine sediment of the Ross Sea, Antarctica, a potential tracer of depositional environment and sediment chronology. Nucl. Instrum. Methods Phys. Res. Sect. B Beam Interact. Mater. Atoms 259, 576–583.
Sproson, A.D., Takano, Y., Miyairi, Y., Aze, T., Matsuzaki, H., Ohkouchi, N., Yokoyama, Y., 2021a. Beryllium isotopes in sediments from Lake Maruwan Oike and Lake Skallen, east Antarctica, reveal substantial glacial discharge during the late Holocene. Quat. Sci. Rev. 256, 106841.
Sproson, A.D., Aze, T., Behrens, B., Yokoyama, Y., 2021b. Initial measurement of beryllium-9 using high-resolution inductively coupled plasma mass spectrometry allows for more precise applications of the beryllium isotope system within the Earth Sciences. Rapid Commun. Mass Spectrom. 35 (8), e9059.
Stone, J.O., Balco, G.A., Sugden, D.E., Caffee, M.W., Sass, L.C., Cowdery, S.G., Siddoway, C., 2003. Holocene deglaciation of Marie Byrd land, west Antarctica. Science 299 (5603), 99–102.
Tessier, A., Campbell, P.G., Bisson, M., 1979. Sequential extraction procedure for the speciation of particulate trace metals. Anal. Chem. 51, 844–851.
The RAISED Consortium, 2014. A community-based geological reconstruction of Antarctic ice sheet deglaciation since the last glacial maximum. Quat. Sci. Rev. Reconstruct. Antarctic Ice Sheet Deglaciation (RAISED) 100, 1–9.
Thomas, R.H., Bentley, C.R., 1978. A model for Holocene retreat of the West Antarctic ice sheet. Quat. Res. 10 (2), 150–170.
Valletta, R.D., Willenbring, J.K., Passchier, S., Elmi, C., 2018. $^{10}Be/^{9}Be$ ratios reflect Antarctic ice sheet freshwater discharge during Pliocene warming. Paleoceanogr. Paleoclimatol. 33, 934–944.
Von Blanckenburg, F., Bouchez, J., 2014. River fluxes to the sea from the ocean's $^{10}Be/^{9}Be$ ratio. Earth Planet Sci. Lett. 387, 34–43.
Von Blanckenburg, F., Bouchez, J., Ibarra, D.E., Maher, K., 2015. Stable runoff and weathering fluxes into the oceans over Quaternary climate cycles. Nat. Geosci. 8, 538.
Wagner, G., Masarik, J., Beer, J., Baumgartner, S., Imboden, D., Kubik, P., Synal, H.-A., Suter, M., 2000. Reconstruction of the geomagnetic field between 20 and 60 kyr BP from cosmogenic radionuclides in the GRIP ice core. Nucl. Instrum. Methods Phys. Res. Sect. B Beam Interact. Mater. Atoms 172, 597–604.
White, D.A., Fink, D., Gore, D.B., 2011. Cosmogenic nuclide evidence for enhanced sensitivity of an East Antarctic ice stream to change during the last deglaciation. Geology 39 (1), 23–26.
White, D.A., Fink, D., Post, A.L., Simon, K., Galton-Fenzi, B., Foster, S., Fujioka, T., Jeromson, M.R., Blaxell, M., Yokoyama, Y., 2019. Beryllium isotope signatures of ice shelves and sub-ice shelf circulation. Earth Planet Sci. Lett. 505, 86–95.
Wittmann, H., Von Blanckenburg, F., Bouchez, J., Dannhaus, N., Naumann, R., Christl, M., Gaillardet, J., 2012. The dependence of meteoric ^{10}Be concentrations on particle size in Amazon River bed sediment and the extraction of reactive $^{10}Be/^{9}Be$ ratios. Chem. Geol. 318, 126–138.
Yamane, M., Yokoyama, Y., Miura, H., Maemoku, H., Iwasaki, S., Matsuzaki, H., 2011. The last deglacial history of Lützow-Holm Bay, East Antarctica. J. Quat. Sci. 26, 3–6.
Yamane, M., Yokoyama, Y., Miyairi, Y., Suga, H., Matsuzaki, H., Dunbar, R.B., Ohkouchi, N., 2014. Compound-specific 14C dating of IODP expedition 318 core U1357A obtained off the Wilkes land coast, Antarctica. Radiocarbon 56, 1009–1017.
Yamane, M., Yokoyama, Y., Abe-Ouchi, A., Obrochta, S., Saito, F., Moriwaki, K., Matsuzaki, H., 2015. Exposure age and ice-sheet model constraints on Pliocene East Antarctic ice sheet dynamics. Nat. Commun. 6 (1), 1–8.
Yamane, M., Yokoyama, Y., Hirabayashi, S., Miyairi, Y., Ohkouchi, N., Aze, T., 2019. Small-to ultra-small-scale radiocarbon measurements using newly installed single-stage AMS at the University of Tokyo. Nucl. Instrum. Methods Phys. Res. Sect. B Beam Interact. Mater. Atoms 455, 238–243.
Yokoyama, Y., Purcell, A., 2021. On the geophysical processes impacting palaeo-sea-level observations. Geosci. Lett. 8 (1), 1–19.
Yokoyama, Y., Anderson, J.B., Yamane, M., Simkins, L.M., Miyairi, Y., Yamazaki, T., Koizumi, M., Suga, H., Kusahara, K., Prothro, L., Hasumi, H., Southon, J.R., Ohkouchi, N., 2016. Widespread collapse of the Ross ice shelf during the late Holocene. Proc. Natl. Acad. Sci. Unit. States Am. 113, 2354.
Yokoyama, Y., Esat, T.M., Thompson, W.G., Thomas, A.L., Webster, J.M., Miyairi, Y., Sawada, C., Aze, T., Matsuzaki, H., Okuno, J.I., Fallon, S., Braga, J.-C., Humblet, M., Iryu, Y., Potts, D.C., Fujita, K., Suzuki, A., Kan, H., 2018. Rapid glaciation and a two-step sea level plunge into the Last Glacial Maximum. Nature 559, 603–607.
Yokoyama, Y., Yamane, M., Nakamura, A., Miyairi, Y., Horiuchi, K., Aze, T., Matsuzaki, H., Shirahama, Y., Ando, Y., 2019a. In-situ and meteoric 10Be and 26Al measurements: improved preparation and application at the University of Tokyo. Nucl. Instrum. Methods Phys. Res. Sect. B Beam Interact. Mater. Atoms.
Yokoyama, Y., Hirabayashi, S., Goto, K., Okuno, J.I., Sproson, A.D., Haraguchi, T., Ratnayake, N., Miyairi, Y., 2019b. Holocene Indian Ocean sea level, Antarctic melting history and past Tsunami deposits inferred using sea level reconstructions from the Sri Lankan, Southeastern Indian and Maldivian coasts. Quat. Sci. Rev. 206, 150–161.
Young, G.M., Nesbitt, H.W., 1998. Processes controlling the distribution of Ti and Al in weathering profiles, siliciclastic sediments and sedimentary rocks. J. Sediment. Res. 68 (3), 448–455.